The SLUGGS survey: measuring globular cluster ages using both photometry and spectroscopy

Christopher Usher [1][*] Jean P. Brodie,[2] Duncan A. Forbes,[3] Aaron J. Romanowsky,[2,4] Jay Strader,[5] Joel Pfeffer [1] and Nate Bastian[1]

[1]*Astrophysics Research Institute, Liverpool John Moores University, 146 Brownlow Hill, Liverpool L3 5RF, UK*
[2]*University of California Observatories, 1156 High Street, Santa Cruz, CA 95064, USA*
[3]*Centre for Astrophysics and Supercomputing, Swinburne University, Hawthorn, VIC 3122, Australia*
[4]*Department of Physics and Astronomy, San José State University, One Washington Square, San Jose, CA 95192, USA*
[5]*Department of Physics and Astronomy, Michigan State University, East Lansing, MI 48824, USA*

ABSTRACT

Globular cluster ages provide both an important test of models of globular cluster formation and a powerful method to constrain the assembly history of galaxies. Unfortunately, measuring the ages of unresolved old stellar populations has proven challenging. Here, we present a novel technique that combines optical photometry with metallicity constraints from near-infrared spectroscopy in order to measure ages. After testing the method on globular clusters in the Milky Way and its satellite galaxies, we apply our technique to three massive early-type galaxies using data from the SAGES Legacy Unifying Globulars and GalaxieS (SLUGGS) survey. The three SLUGGS galaxies and the Milky Way show dramatically different globular cluster age and metallicity distributions, with NGC 1407 and the Milky Way showing mostly old globular clusters, while NGC 3115 and NGC 3377 show a range of globular ages. This diversity implies different galaxy formation histories and that the globular cluster optical colour–metallicity relation is not universal as is commonly assumed in globular cluster studies. We find a correlation between the median age of the metal-rich globular cluster populations and the age of the field star populations, in line with models where globular cluster formation is a natural outcome of high-intensity star formation.

Key words: globular clusters: general – galaxies: evolution – galaxies: star clusters: general – galaxies: stellar content.

1 INTRODUCTION

Globular clusters (GCs) have long held promise as probes of galaxy formation and evolution (see reviews by Brodie & Strader 2006; Forbes et al. 2018). Found in virtually all galaxies with stellar masses above 10^9 $M_\odot$ and in most above 10^8 $M_\odot$, the high surface brightnesses of GCs allow the old and intermediate age populations of galaxies to be studied at much greater distances than with individual stars. Since most GCs in the Milky Way (MW) are old ($\gtrsim 11$ Gyr; e.g. Dotter et al. 2010; VandenBerg et al. 2013), GCs are commonly seen as fossils of the earlier stages of galaxy formation. The properties of GCs observed today reflect both the conditions of GC formation but also the physics of GC survival since GCs lose mass and may even be destroyed by tidal interactions (e.g. Elmegreen 2010; Kruijssen 2015; Li & Gnedin 2019). As such,

by understanding how GCs form and evolve, we can extend our understanding of how individual galaxies form and evolve.

GC age distributions provide both a powerful test of GC formation models and a potentially important way to study galaxy assembly. Two broad classes of models have been proposed for GC formation. In the first class of models (e.g. Peebles 1984; Katz & Ricotti 2014; Trenti, Padoan & Jimenez 2015; Chiou et al. 2019) GC formation requires the special conditions of the early Universe, forming before or during the epoch of reionization ($z \gtrsim 6$). In the second class (e.g. Elmegreen & Efremov 1997; Muratov & Gnedin 2010; Shapiro, Genzel & Förster Schreiber 2010; Kruijssen 2015; Li et al. 2017; Choksi, Gnedin & Li 2018; Kim et al. 2018; Ma et al. 2019), GC formation is the natural outcome of intense star formation and GC formation should consequently peak just before the peak of cosmic star formation at redshift $z \sim 2$ (El-Badry et al. 2019; Reina-Campos et al. 2019). In the first class of models, GC ages should sharply peak around 13 Gyr and show relatively little variance galaxy-to-galaxy; in the second the age distribution should be broader and

both the width and position of the peak should vary with galaxy assembly history (e.g. Kruijssen et al. 2019a).

Following a long history of using the GC system of the MW to understand its formation (e.g. Searle & Zinn 1978; Forbes & Bridges 2010; Leaman, VandenBerg & Mendel 2013), Kruijssen et al. (2019b) used the ages and metallicities of GCs in the MW together with predictions of the cosmological MOdelling Star cluster population Assembly In Cosmological Simulations within EAGLE (E-MOSAICS) simulations (Pfeffer et al. 2018; Kruijssen et al. 2019a) of galaxy and GC system formation to reconstruct in detail the assembly history of the MW. Kruijssen et al. (2019b) placed strong constraints on the number, masses, and redshifts of mergers that built up the MW and found that the MW assembled earlier than average for a galaxy of its mass. While studies of the MW are important, it is only a single galaxy with a formation history that is likely atypical of a galaxy of its mass and environment (e.g. Mackereth et al. 2018). To test whether models for GC and galaxy formation reproduce the diverse population of galaxies we observe today, we need to extend GC stellar population studies to a wider range of galaxies.

Beyond the Local Group, GCs must be studied via their integrated light. Unfortunately, the ages of old stellar populations are difficult to measure reliably from integrated light. Optical colours suffer from a strong age–metallicity degeneracy (e.g. Worthey 1994). Adding near-infrared photometry can in principle break this degeneracy, although observing deep enough photometry over a wide area is challenging and has had limited success (e.g. Puzia et al. 2002; Hempel et al. 2003; Larsen, Brodie & Strader 2005; Chies-Santos et al. 2011). Extragalactic GC ages have typically been measured using optical spectroscopy in the regions of the Hβ and Mgb spectral features. Unfortunately, the high signal-to-noise ratio spectra required to disentangle the effects of age, metallicity, and chemistry have limited these studies to relatively small samples of GCs. These studies (e.g. Cohen, Blakeslee & Ryzhov 1998; Forbes et al. 2001; Puzia et al. 2005; Strader et al. 2005; Norris et al. 2008) have generally found old ages (∼12 Gyr) but evidence of younger GCs has been seen in a few galaxies (e.g. Chandar et al. 2006; Sharina, Afanasiev & Puzia 2006; Beasley et al. 2008; Chomiuk, Strader & Brodie 2008; Martocchia et al. 2018; Sesto et al. 2018). A major systematic uncertainty for integrated light ages remains the horizontal branch (HB). Stellar population models have trouble reproducing the ages of MW GCs with blue HBs (e.g. Worthey 1994; Maraston & Thomas 2000; Schiavon 2007; Conroy et al. 2018) as the presence of hot HB stars can mimic the appearance of a hotter (younger) main sequence turn-off.

In Usher et al. (2015), we found clear evidence that the relationship between optical colour and the strength of the near-infrared calcium triplet (CaT) spectral feature varies between galaxies. This suggests the stellar populations of GCs vary between galaxies (see also Powalka et al. 2016; Villaume et al. 2019). Recently Usher et al. (2019) studied the behaviour of the CaT in GCs in the MW and its satellite galaxies and found that neither age nor HB morphology has a measurable effect on the measured CaT strength for GCs older than a couple of Gyr. By combining the age-independent metallicity measurement from the CaT with optical photometry that is sensitive to both age and metallicity, we can break the degeneracy and measure both GC ages and metallicities. In this paper, we test this technique on GCs in the MW and its satellite galaxies (Section 2) before applying it to three massive early-type galaxies from the SAGES Legacy Unifying Globulars and GalaxieS (SLUGGS) survey (Brodie et al. 2014) (Section 3), and discussing our results in Section 4.

2 AGES FROM COMBINING PHOTOMETRY AND SPECTROSCOPY

To measure the ages of our GCs, we fit our photometry with stellar population synthesis models while using our CaT-based [Fe/H] measurements as a constraint. We used stellar population model grids calculated with version 3.0 of Flexible Stellar Population Synthesis (FSPS) code (Conroy, Gunn & White 2009; Conroy & Gunn 2010) using the MIST stellar isochrones (Choi et al. 2016), the MILES spectral library (Sánchez-Blázquez et al. 2006), and a Kroupa (2001) initial mass function. These models were calculated at [Fe/H] = [−3.0, −2.5, −2.0, −1.75, −1.50, −1.25, −1.00, −0.75, −0.50, −0.25, +0.0, +0.5] and at ages between 0.1 and 15.8 Gyr in intervals of 0.05 dex.

Similarly to Leja et al. (2017) we performed a two-step process to find the posterior distribution of our model for each GC. First, we performed a coarse grid search in age and metallicity, calculating the best-fitting mass for each age and metallicity given the input $E(B − V)$ reddening. Second, we used version 2.2.1 of the Markov chain Monte Carlo (MCMC) code EMCEE (Foreman-Mackey et al. 2013) with 1000 walkers, 100 burn-in steps, and 500 production steps to sample the posterior distribution. We sampled the posteriors of age (assuming a flat prior between 0.1 and 15.8 Gyr), metallicity (assuming a flat prior between [Fe/H] = −3.0 and +0.7), stellar mass (assuming a flat prior in log mass), and reddening (assuming a Gaussian prior) subject to the constraints provided by each of the photometry bands and the CaT [Fe/H] measurements that are each assumed to be normally distributed. We initialized the walkers in a small ball around the best-fitting age, metallicity, and mass from the grid search. Because of the multimodal nature of the likelihood function, we utilized the EMCEE parallel-tempered ensemble sampler rather than the default affine-invariant ensemble sampler. When sampling the likelihood we linearly interpolated between the model grid points. To correct for the effects of extinction we used the reddenings provided by Schlafly & Finkbeiner (2011) for a $R_V = 3.1$ reddening law. Our assumption of simple stellar populations is appropriate for GCs but may not be valid for stripped galactic nuclei (e.g. ω Cen, M54) that often show large metallicity spreads and extended star formation histories (e.g. Layden & Sarajedini 2000; Carretta et al. 2010; Johnson & Pilachowski 2010; Villanova et al. 2014).

In this work, we have used a relatively simple metallicity prior based on an empirical relationship between CaT strength and metallicity when fitting the photometry. Our technique could be easily extended to use a more sophisticated age–metallicity (and possibly chemistry) prior from full spectral fitting (e.g. Koleva et al. 2008; Larsen, Brodie & Strader 2017; Wilkinson et al. 2017; Conroy et al. 2018) or even by simultaneously fitting both photometry and spectroscopy to fully utilize the information contained in the spectroscopy (Leja et al. 2017). A previous example of combining the stellar population constraints from optical photometry and spectroscopy can be found in Gu et al. (2018) who used both to place stronger constraints on the old ages of three ultradiffuse galaxies.

2.1 Tests on the Local Group globular clusters

We test our method on observations of GCs in the MW and its satellite galaxies. We use [Fe/H] measurements calculated from the CaT measurements given in table 5 of Usher et al. (2019) and equation (1) of Usher et al. (2019). We note that the Usher et al. (2019) measurements were made using the same code and
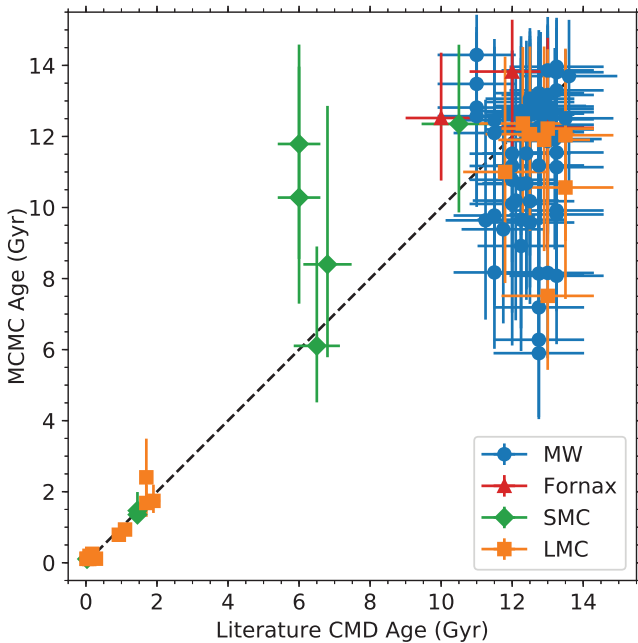
Figure 1. Medians of the Markov chain Monte Carlo (MCMC) age posteriors versus literature ages for globular clusters (GCs) in the Milky Way (MW; blue circles), the Large Magellanic Cloud (LMC; orange squares), the Small Magellanic Cloud (SMC; green diamonds), and the Fornax dwarf spheroidal (red triangles). The dashed line is the one-to-one line. There is relatively good agreement for GCs of all ages both in the MW and in its satellite galaxies.

similar resolution spectra to our SLUGGS DEep Imaging Multi-Object Spectrograph (DEIMOS) spectra. For the MW GCs we use the *BVRI* photometry from the 2010 edition of the Harris (1996, 2010) catalogue, for the GCs in the Large and Small Magellanic Clouds (LMC and SMC) we use the *BV* photometry from van den Bergh (1981), and for the Fornax dwarf spheroidal GCs we use the *BV* photometry from van den Bergh (1969). We note that ($B - V$) and ($g - r$) show similar behaviour with age and metallicity, while the colours ($V - R$), ($R - I$), ($r - i$), and ($i - z$) all show similar behaviour to one another. Following van den Bergh (1981) we estimate an uncertainty of 0.02 mag in each of the photometric bands. As in Usher et al. (2019), we remove from our sample GCs whose CaT observations are based on observations with apertures enclosing less than 5×10^3 M$_\odot$ in order to reduce stochastic effects. We use the reddening values from Usher et al. (2019) and assume the reddening uncertainty to be 0.02 mag added in quadrature with one-tenth of the reddening.

We plot the posterior distributions of one of our MW GCs (NGC 5272) in Fig. A1 and a comparison of the medians of our age posteriors to literature ages (from resolved colour–magnitude diagrams) in Fig. 1. The sources of these ages are given in table 1 of Usher et al. (2019) and we refer the interested reader to section 2 of Usher et al. (2017) for further details. For the MW GCs, these ages are mostly from Dotter et al. (2010) and Dotter, Sarajedini & Anderson (2011) or were derived in a similar way (Milone et al. 2014). The satellite galaxy GC ages are from a range of sources including Geisler et al. (1997), Olsen et al. (1998), Glatt et al. (2008), Goudfrooij et al. (2014), Niederhofer et al. (2015), and de Boer & Fraser (2016). In general, we see good agreement between our MCMC age constraints and literature ages. Because of the upper limit on the age prior of 15.8 Gyr, the age posteriors of

old GCs can extend to significantly younger ages than older ages. At ages of ∼2 Gyr and younger, where the CaT is a less reliable metallicity indicator (Usher et al. 2019), our technique still returns ages reliable at the 500 Myr level. We note that at these ages the colours are relatively less sensitive to metallicity. When the CaT metallicities show the largest discrepancies with the literature, the CaT metallicities are overestimated and result in younger ages. The difference in our ages and literature ages shows no relationship with GC age, metallicity, mass, or reddening. Neither is there any significant correlation between the age difference and the HB parameter $\Delta(V - I)$ of Dotter et al. (2010) (a Kendell's τ of -0.12 for a p-value of 0.32) nor between the HB parameters $L1$ and $L2$ of Milone et al. (2014) ($\tau = -0.06$ and -0.15, respectively, for $p = 0.64$ and 0.21). We note that the main limiting factor of these comparisons is the quality of the photometry and of the reddening correction as the uncertainties on the CaT metallicities are significantly smaller.

3 APPLYING THE TECHNIQUE TO SLUGGS GALAXY GLOBULAR CLUSTERS

We apply our MCMC age–metallicity technique to GCs around three galaxies from the SLUGGS survey – NGC 1407, NGC 3115, and NGC 3377. NGC 1407 is a slowly rotating E0 galaxy with a stellar mass of 4×10^{11} M$_\odot$, NGC 3115 is a fast rotating S0 galaxy with a stellar mass of 9×10^{10} M$_\odot$, and NGC 3377 is an E5/6 galaxy with an embedded disc and a stellar mass of 3×10^{10} M$_\odot$ (Arnold et al. 2014; Forbes et al. 2017b). For the GCs in these three galaxies we use Subaru Suprime-Cam *gri* photometry presented in Pota et al. (2013) for NGC 1407 and NGC 3377 and in Arnold et al. (2011) for NGC 3115 and assume an uncertainty in the reddening of $E(B - V) = 0.01$ mag for these GCs. We use the Keck DEIMOS spectra presented in Forbes et al. (2017a) and use the code described in Usher et al. (2019) to measure the CaT strengths before using the empirical relation derived by Usher et al. (2019) to convert them into [Fe/H]. For GCs obtained in the SLUGGS survey, the photometric and reddening uncertainties are smaller than for the MW GCs, but the uncertainties on the CaT metallicities are larger. We plot the colours, magnitudes, and CaT strengths of GCs in the three SLUGGS galaxies and the MW in Fig. 2 and provide an example posterior distribution for one of the SLUGGS GCs in Fig. A2.

In Fig. 3, we compare our MCMC age measurements with literature age measurements in NGC 1407 (Cenarro et al. 2007) and in NGC 3115 (ages measured by Norris, Sharples & Kuntschner 2006 using measurements from Kuntschner et al. 2002). Both Norris et al. (2006) and Cenarro et al. (2007) measured ages by χ^2 minimization of the measured Lick indices (Worthey et al. 1994) and the stellar population models of Thomas, Maraston & Bender (2003) and Thomas, Maraston & Korn (2004). We find good agreement between our age constraints and the literature measurements with the largest disagreement coming from a GC we measure to be old ($13.8^{+1.3}_{-2.0}$ Gyr) but measured to be young by Cenarro et al. (2007, 3.5 ± 0.8 Gyr) but suggested by Cenarro et al. (2007) to be an old GC with a blue HB.

We plot the age–metallicity posterior distributions for the three galaxies and our measurements of MW GCs in Fig. 4. The four galaxies show wildly different GC age–metallicity distributions. NGC 1407 shows both an old unimodal age distribution (with a possible tail to intermediate ages) and a unimodal metallicity distribution. NGC 3115 shows broad age and metallicity distributions with a clear separation between a metal-poor age–metallicity sequence and a metal-rich sequence. NGC 3377 shows broad age
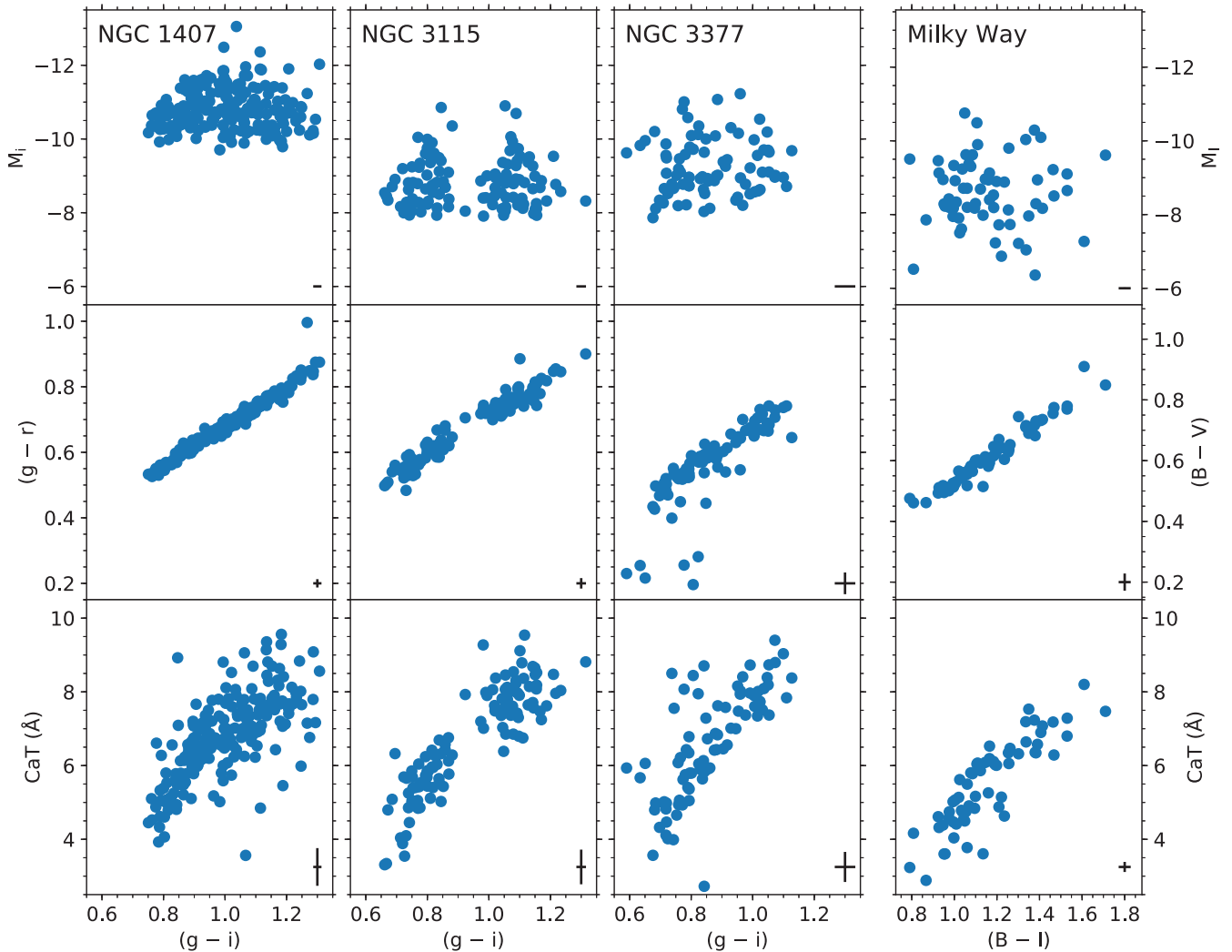
Figure 2. Top row: colour–magnitude diagrams of our GCs in the three SLUGGS galaxies and the MW. Middle row: colour–colour plots for the four galaxies. Bottom row: colour–CaT strength plots for four galaxies. In the lower left of each of the panels the median uncertainties are plotted. The ranges of $(B - V)$, $(B - I)$, and M_I for the MW correspond to the same range of $(g - r)$, $(g - i)$, and M_i for the other three galaxies. There are significant differences in the colour and CaT distributions of the four galaxies. The GCs in NGC 1407 are significantly more luminous than those in other galaxies. The luminosity distributions of the other galaxies are similar to one another, although the MW sample extends to fainter GCs.

and metallicity distributions with a clear age–metallicity sequence. The MW shows an old unimodal age distribution and a broad metallicity distribution. For NGC 3115, NGC 3377, and the MW, the mass distributions are broadly similar with median GC masses of $\sim 4 \times 10^5$ $M_\odot$ and an interquartile range spanning a factor of ~ 3. The more distant NGC 1407 sample, however, has a higher median mass of $\sim 3 \times 10^6$ $M_\odot$. Since NGC 1407 displays a strong blue tilt (Harris et al. 2006; Harris 2009), our sample of GCs is deficient in metal-poor GCs compared to the galaxy as a whole (see figs 1c and 12 in Usher et al. 2012). Red GCs are slightly over-represented in our NGC 3377 sample (see fig. 1f in Usher et al. 2012), while the colour distribution of GCs with CaT metallicities closely traces the entire population in NGC 3115 (see fig. 1e in Usher et al. 2012). The literature metallicity distribution of our sample of MW GCs is consistent with being drawn from the metallicity distribution of the 2010 edition of the Harris (1996, 2010) catalogue.

By sampling the age posterior distributions we calculate the median ages of each galaxy's GCs that we give in Table 1 and GCs more or less metal poor than [Fe/H] = −0.8 in each galaxy. [Fe/H] = −0.8

is close to the median metallicities of our samples of NGC 3115 and NGC 3377 and neatly dividing the two age–metallicity sequences in NGC 3115. If we use the median metallicities for each galaxy's GCs, we get identical median ages for the two subpopulations as for the [Fe/H] = −0.8 split. The median ages of the different galaxy populations and metallicity subpopulations reinforce the diversity of age distributions. NGC 3377 has the youngest median age, while NGC 1407 and the MW have the oldest. In both NGC 1407 and the MW the ages of the two metallicity subpopulations are consistent, in contrast to NGC 3115, where the metal-poor GCs are slightly younger than the metal-rich ones, and to NGC 3377, where the metal-rich GCs are significantly younger than the metal-poor ones. At high metallicity NGC 1407's and the MW's GCs are mostly old, NGC 3115 spans a wide range of ages and NGC 3377 metal-rich GCs appear mostly young. At lower metallicities the differences between galaxies are less obvious but unlike the other galaxies NGC 3377 shows evidence for a handful of ~ 2 Gyr GCs at [Fe/H] ~ -1. Despite NGC 3115 and NGC 3377 showing consistent metallicity distributions [a Kolmogorov–Smirnov (KS) test returns
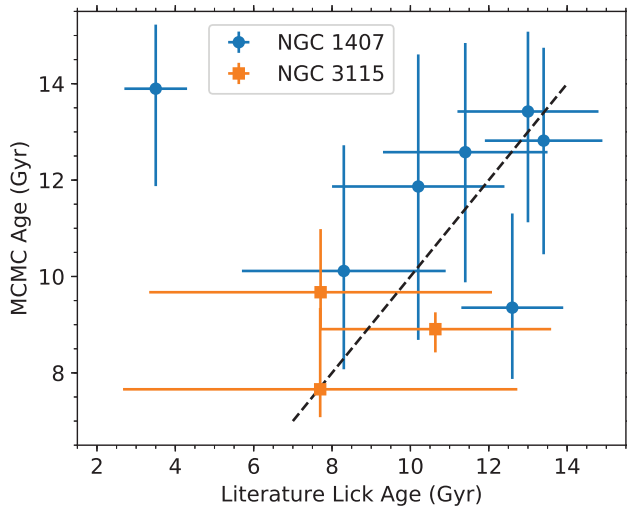
Figure 3. Medians of the MCMC age posteriors versus literature ages for GCs in NGC 1407 (blue circles, from Cenarro et al. 2007) and NGC 3115 (orange squares, from Kuntschner et al. 2002; Norris et al. 2006). The dashed line is the one-to-one line. There is relatively good agreement for GCs in both galaxies. The one NGC 1407 GC with a young literature age was suggested by Cenarro et al. (2007) to be an old GC with a blue HB in agreement with the median of our age posterior.

a p-value of 0.55], the two galaxies show strongly inconsistent age distributions (a KS test p-value of 1×10^{-6}). This highlights the importance of age in studying the formation history of these GCs systems; an analysis based solely of metallicity would conclude the two GC systems were similar. On the other hand, the MW and NGC 1407 show similar age distributions (a KS test p-value of 0.46), but the NGC 1407 GCs are on average much more metal rich, even after accounting for the effects of NGC 1407's blue tilt.

4 DISCUSSION

The good agreement between our Local Group GC ages and literature ages (see Fig. 1) indicates that the effects of HB morphology or non-solar abundance ratios on our ages are likely relatively small. In the MW and other galaxies, there is a strong correlation between the morphology of the HB and GC mass at fixed metallicity, with more massive GCs having bluer HBs (e.g. Recio-Blanco et al. 2006; Gratton et al. 2010; Peacock et al. 2017, 2018). This correlation is likely due to a correlation between GC mass and the internal spread of He abundance, with more massive GCs having larger ranges of He abundance (e.g. D'Antona et al. 2002; Milone et al. 2018). Thus, the relative ages of GCs of similar masses should be reliable, suggesting that the differences between the NGC 3115, NGC 3377, and MW age distributions are real. If our ages were significantly affected by the morphology of the HB, we would expect the more massive GCs in NGC 1407 to appear younger yet their ages are consistent with those in the MW. We plan to quantify the effects of HB morphology and different abundance patterns on our ages in future work. We note that our ages are likely more reliable in a relative sense than absolute, especially at fixed metallicity. Our GC age and metallicity measurements are also in agreement with previous spectroscopic studies (see Fig. 3) in the blue of NGC 3115 (Kuntschner et al. 2002; Norris et al. 2006) and NGC 1407 (Cenarro et al. 2007) and qualitatively with the optical–near-infrared imaging study of NGC 3377 by Chies-Santos et al. (2011). We note that our samples are ∼10× larger than the previous spectroscopic studies

of these galaxies and achieved with significantly shorter exposure times (∼2 h per mask for our observations compared to 3.5 h for Kuntschner et al. 2002 and 7 h for Cenarro et al. 2007).

The diversity in GC ages and metallicities both within and between galaxies agrees with the range of colour–CaT relationships observed by Usher et al. (2015), the variation in colour–metallicity relationship seen by Villaume et al. (2019), and by the variation in GC colour–colour relationship with environment seen by Powalka et al. (2016). Further evidence for this diversity in stellar populations is seen with the various age distributions observed in previous spectroscopic studies that find uniformly old ages in some galaxies (e.g. NGC 1399, Forbes et al. 2001; NGC 4365, Brodie et al. 2005; Chies-Santos, Larsen & Kissler-Patig 2012) but not others (e.g. NGC 1316, Goudfrooij et al. 2001; Sesto et al. 2018; NGC 5128, Peng, Ford & Freeman 2004; Beasley et al. 2008). This diversity implies that a single colour–metallicity relation is not a good description of most GC systems as has been assumed by most previous studies. In particular, the assumption that different mass galaxies follow the same colour–metallicity relationship is incorrect since lower mass galaxies tend to host younger GCs (e.g. Chandar et al. 2006; Sharina et al. 2006; Mora, Larsen & Kissler-Patig 2008; Parisi et al. 2014; this work).

4.1 Galaxy assembly histories

We can qualitatively interpret the assembly histories of the three SLUGGS galaxies using the framework of Kruijssen et al. (2019a) in an analogous manner to the study of the MW by Kruijssen et al. (2019b) using the E-MOSAICS simulations (Pfeffer et al. 2018; Kruijssen et al. 2019a).[1] As described by Kruijssen et al. (2019a), the evolution of the stellar age–metallicity relation of galaxies (as predicted by cosmological simulations such as EAGLE; Crain et al. 2015; Schaye et al. 2015) can be used to estimate what mass of galaxy a GC of a given age and metallicity likely formed in. By using the evolution of galaxies in age–metallicity space, it is possible to connect GCs to a likely progenitor. The GCs associated with the most massive progenitor can be linked to the *in situ* population, while the GCs associated with lower mass progenitors were likely accreted. The youngest GC associated with a particular lower mass progenitor places an upper limit on when that progenitor was accreted as cluster formation halts in the lower mass progenitor when it is accreted. By using the observed scaling between the number of GCs and host galaxy halo mass (e.g. Blakeslee, Tonry & Metzger 1997; Spitler & Forbes 2009; Harris, Blakeslee & Harris 2017) it is possible to estimate the number of GCs formed by a galaxy with a given age and metallicity. By comparing this expected number with the observed number of GCs, the number of progenitors of a given mass can be estimated. As noted by Kruijssen et al. (2019a), this analysis is most sensitive to unequal mass mergers between redshifts of $z = 1$ and 2.5 where the accreted galaxies are massive enough to form GCs (stellar masses of ∼10^8 M$_\odot$ and above). Above a redshift of $z = 2.5$, the steep age–metallicity relations of different masses galaxies become difficult to distinguish from one another especially with realistic age uncertainties, while below $z = 1$ cosmic GCs formation declines rapidly (Reina-Campos et al. 2019).

---

[1]The analysis of Kruijssen et al. (2019a,b) was tailored to central MW mass galaxies but the general principles should be applicable to any galaxy massive enough to host a populous GC system.
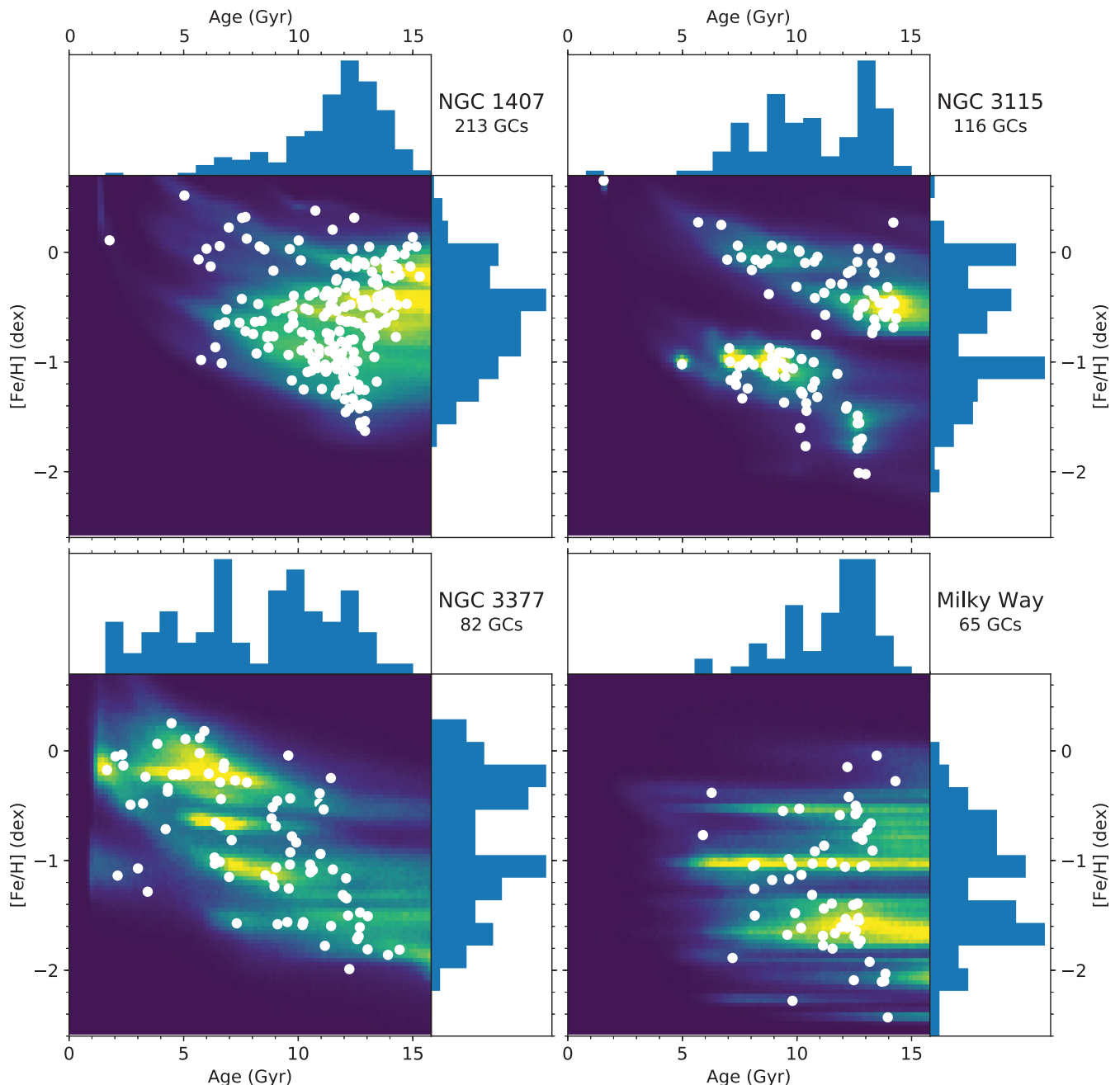
Figure 4. Age–metallicity posterior distribution for GCs around three SLUGGS galaxies and the MW. The 2D histograms show the sum of the individual age–metallicity posterior distributions, while the white points and the 1D histograms show the medians of the age and metallicity posteriors for each GC. The four galaxies show wildly different GC age and metallicity distributions, suggesting different formation histories. We note that the photometric and reddening uncertainties are generally larger for the MW GCs than for the SLUGGS GCs, while the CaT metallicities are smaller for the MW GCs than for the SLUGGS ones.

4.1.1 NGC 1407

Most GCs of NGC 1407 are old (ages >10 Gyr). It implies that NGC 1407 formed most of its stellar mass early. The likely tail to younger ages in NGC 1407 suggests that NGC 1407 assembled over an extended period of time, while the wide range of metallicities of these younger GCs suggests NGC 1407 was built from a wide range of mass progenitors. We note that the age uncertainties of our NGC 1407 GCs are smaller than in the MW due to the smaller uncertainties on the NGC 1407 photometry and reddening. Stellar population studies of NGC 1407's field star population (e.g. Spolaor et al. 2008; Johnston et al. 2018; Ferré-Mateu et al. 2019) paint a

consistent picture with old ages (11–13 Gyr) and high [α/Fe] values (suggestive of rapid star formation). The kinematics (e.g. Oser et al. 2010; Arnold et al. 2014; Johnston et al. 2018; Ferré-Mateu et al. 2019) and the strong field star metallicity gradient (Spolaor et al. 2008; Pastorello et al. 2014; Ferré-Mateu et al. 2019) are suggestive of a large accretion fraction for NGC 1407's stellar mass. This is in line with cosmological simulations of galaxy formation (e.g. Oser et al. 2010; Rodriguez-Gomez et al. 2016; Qu et al. 2017; Forbes & Remus 2018) that predict the most massive galaxies, such as the brightest group galaxy NGC 1407, form most of their stellar mass early but assemble their mass late.

Table 1. GC age medians.

Galaxy	Full		[Fe/H] < -0.8		[Fe/H] > -0.8	
	Gyr	N	Gyr	N	Gyr	N
NGC 1407	$11.9^{+0.3}_{-0.3}$	213	$11.7^{+0.4}_{-0.4}$	74	$12.0^{+0.3}_{-0.3}$	139
NGC 3115	$10.9^{+0.4}_{-0.4}$	116	$9.7^{+0.5}_{-0.4}$	56	$12.3^{+0.5}_{-0.5}$	60
NGC 3377	$8.0^{+0.5}_{-0.4}$	82	$10.3^{+0.7}_{-0.7}$	42	$6.1^{+0.5}_{-0.5}$	40
Milky Way	$11.7^{+0.5}_{-0.6}$	65	$11.6^{+0.6}_{-0.6}$	48	$12.1^{+1.0}_{-1.1}$	17

4.1.2 NGC 3115

The two age–metallicity sequences of NGC 3115 can be identified with a more metal-rich population that formed *in situ* and a more metal-poor population that formed either in lower mass galaxies that merged with NGC 3115 or from gas that was brought in by lower mass galaxies accreting on to NGC 3115. The two sequences span similar age ranges, although the *in situ* GCs likely formed earlier on average than the accreted GCs. The large, clear gap in metallicity between the two sequences suggests a substantial difference in stellar mass between the progenitors. The roughly equal numbers of metal-poor and metal-rich GCs suggest equal contributions from *in situ* and accreted GCs under the assumption that the low-metallicity branch is dominated by accreted GCs, although some fraction of the old metal-poor GCs likely formed *in situ*. Since the number of GCs scales with galaxy mass, this suggests a number of lower mass galaxies were accreted on to NGC 3115 to build up its GC system. The ages of the *in situ* GCs show agreement with studies of NGC 3115's field star populations (Norris et al. 2006; Guérou et al. 2016; Poci et al. 2019) with an old (10–13 Gyr), α-enhanced spheroid and a disc with a star-forming history declining from a peak at old ages to 5 Gyr and younger. The bimodal nature of NGC 3115 formation is supported by the bimodal halo star metallicity distribution measured by Peacock et al. (2015), with the peaks of the halo field star distribution coinciding with those of the GCs. The *in situ* build up of NGC 3115 bulge and disc without late major mergers and the build up of NGC 3115's halo by many minor mergers are supported by the joint stellar population–dynamical study of Poci et al. (2019).

4.1.3 NGC 3377

The large age spread in NGC 3377 GCs suggests an extended formation history, while the lack of old, metal-rich GCs compared to the other SLUGGS galaxies and the MW suggests a late peak in its star formation history relative to the other galaxies in this study. However, the peak of GC formation is close to the expected peak of star formation for a galaxy of its mass (e.g. Qu et al. 2017). The wide range of metallicities at intermediate ages shows the contribution of accreted galaxies with the trio of GCs with ages of ~4 Gyr and metallicity of [Fe/H] ~ -1.2 suggests the relatively recent accretion of a dwarf galaxy. In agreement with wide range GC ages in NGC 3377, McDermid et al. (2015) measured a luminosity weighted age of 7 ± 1 Gyr and a mass weighted age of 11 ± 1 Gyr for the field star population of NGC 3377.

4.1.4 Milky Way

The assembly history of the MW has already been studied using its GC ages and metallicities by Kruijssen et al. (2019b) and we do not attempt to repeat their analysis here. We do note that within our admittedly large uncertainties, our age and metallicity

measurements agree with literature age–metallicity relationships for the MW (e.g. Forbes & Bridges 2010; Dotter et al. 2011; Leaman et al. 2013; Kruijssen et al. 2019b). Kruijssen et al. (2019b) concluded that the MW assembled relatively early for a galaxy of its mass, in line with the evidence from the MW's field stars (e.g. Snaith et al. 2014; Mackereth et al. 2018). The prediction by Kruijssen et al. (2019b) that the MW's accretion history has been dominated by three relatively massive galaxies has been supported with the association of a large number of the MW GCs with a similar number of progenitors identified in *Gaia* and earlier data (e.g. Massari et al. 2017; Helmi et al. 2018; Myeong et al. 2018, 2019; Sohn et al. 2018; Massari, Koppelman & Helmi 2019). The ages and metallicities of the MW's halo and thick disc stars (e.g. Schuster et al. 2012; Gallart et al. 2019) show good agreement with the literature values for MW GCs. The large population of young and intermediate age GCs in the Magellanic Clouds is also consistent with the star formation history in these galaxies (e.g. Carrera et al. 2008; Harris & Zaritsky 2009; Parisi et al. 2014; Bastian & Niederhofer 2015).

Taken together the assembly histories implied by the age–metallicity distributions of the four galaxies agree with the evidence from other observables. The median ages of the metal-rich GCs in the three SLUGGS galaxies (12.0 ± 0.3, 12.3 ± 0.5, and 6.1 ± 0.5 Gyr for NGC 1407, NGC 3115, and NGC 3377, respectively) agree well with the ages of the majority of field stars (11–13, 10–13, and 7–11 Gyr, respectively), implying that the metal-rich GCs in these galaxies formed on average at the same time as most of the field stars. Since the ratio of mass in GCs to field star mass at fixed metallicity strongly declines with increasing metallicity (e.g. Harris & Harris 2002; Larsen, Strader & Brodie 2012; Lamers et al. 2017), we expect the ages of the metal-rich GCs to more closely trace the field star age distribution than the ages of all GCs. This agreement supports models of GC formation (e.g. Kruijssen 2015; Li et al. 2017; Pfeffer et al. 2018; Ma et al. 2019) where GC formation is the natural outcome of intense star formation and galaxies with high star formation rates at later times can form younger GCs (Kruijssen 2015). Since the GC formation is biased to the most intense period of star formation and the population of GCs we observe today is the product of both GC formation and destruction, while we expect a connection between the field star age distribution and the GC age distribution, we do not expect that the GC age distribution to be exactly the same as the field star age distribution in an analogous manner to the relationship between the GC metallicity distribution and the field star metallicity distribution. The range of ages we observe in both metal-poor and metal-rich GCs indicates that GC formation is a process that occurs across cosmic time and rules out models that predict that GC formation requires special conditions in the early Universe. The ongoing formation of GCs is observed today with the formation of young, massive star clusters in galaxies with extreme star formation rates (e.g. Holtzman et al. 1992; Whitmore et al. 1993; Maraston et al. 2004; Bastian et al. 2006; Portegies Zwart, McMillan & Gieles 2010).

The lowest mass galaxy of the three SLUGGS galaxies (NGC 3377) has the youngest GCs on average, while the most massive (NGC 1407) has the oldest GCs is in line with galactic downsizing (e.g. Bower, Lucey & Ellis 1992; Cowie et al. 1996; Thomas et al. 2005; Fontanot et al. 2009), although there is a diversity of galaxy assembly histories at fixed stellar mass. This diversity at fixed stellar masses is illustrated by the fact that the MW hosts an older GC system on average than NGC 3115 or NGC 3377 despite its stellar mass (6×10^{10} M$_\odot$; e.g. Bland-Hawthorn & Gerhard 2016) is between the SLUGGS galaxies (9×10^{10} and 3×10^{10} M$_\odot$, respectively). Understanding how much scatter exists

in the age distributions of GC systems and how much variation in galaxy assembly histories exists, both with stellar mass and at fixed mass, requires a larger sample of galaxies.

5 CONCLUSIONS

In this work we have used a novel technique to combine age-independent metallicities from the CaT with optical photometry to measure the ages of GCs around the MW and three galaxies from the SLUGGS survey. We find good agreement between our ages and those from literature (Figs 1 and 3). We find a diversity of age–metallicity distributions, implying different galaxy assembly histories (Fig. 4). We note that both ages and metallicities are required to distinguish between different formation histories as galaxies with similar metallicity distributions can have wildly different age distributions (e.g. NGC 3115 and NGC 3377). The assumption that all GCs in all galaxies follow the same colour–metallicity relationship, long used in extragalactic GC studies, needs to be discarded. Our observed connection between the median metal-rich GC age and field star age shows GC formation traces the peaks of star formation. We observe a wide range of GCs ages, demonstrating that GC formation is a process ongoing to the present day. Taken together, these findings support models where GC formation is a natural outcome of star formation and reject models where GC formation requires special conditions in the early Universe. We used the age–metallicity distributions of the three SLUGGS galaxies to study their formation and assembly histories. We find that NGC 1407 formed its stellar mass early but had an extended assembly history, NGC 3115's assembly was dominated by a number of unequal mass mergers, and NGC 3377 formed its stellar mass relatively late, as expected for a galaxy of its stellar mass. In future work, we will extend this age–metallicity analysis to the remaining SLUGGS galaxies. We will quantitatively compare the observed age–metallicity distributions with the simulated GC systems of galaxies with the same stellar masses from E-MOSAICS and from other cosmological models of GC formation in order to constrain the assembly histories of the SLUGGS galaxies.

REFERENCES

Arnold J. A., Romanowsky A. J., Brodie J. P., Chomiuk L., Spitler L. R., Strader J., Benson A. J., Forbes D. A., 2011, ApJ, 736, L26
Arnold J. A. et al., 2014, ApJ, 791, 80
Astropy Collaboration et al., 2013, A&A, 558, A33
Bastian N., Niederhofer F., 2015, MNRAS, 448, 1863
Bastian N., Saglia R. P., Goudfrooij P., Kissler-Patig M., Maraston C., Schweizer F., Zoccali M., 2006, A&A, 448, 881
Beasley M. A., Bridges T., Peng E., Harris W. E., Harris G. L. H., Forbes D. A., Mackie G., 2008, MNRAS, 386, 1443
Blakeslee J. P., Tonry J. L., Metzger M. R., 1997, AJ, 114, 482
Bland-Hawthorn J., Gerhard O., 2016, ARA&A, 54, 529
Bower R. G., Lucey J. R., Ellis R. S., 1992, MNRAS, 254, 601
Brodie J. P., Strader J., 2006, ARA&A, 44, 193
Brodie J. P., Strader J., Denicoló G., Beasley M. A., Cenarro A. J., Larsen S. S., Kuntschner H., Forbes D. A., 2005, AJ, 129, 2643
Brodie J. P. et al., 2014, ApJ, 796, 52
Carrera R., Gallart C., Hardy E., Aparicio A., Zinn R., 2008, AJ, 135, 836
Carretta E. et al., 2010, A&A, 520, A95
Cenarro A. J., Beasley M. A., Strader J., Brodie J. P., Forbes D. A., 2007, AJ, 134, 391
Chandar R., Puzia T. H., Sarajedini A., Goudfrooij P., 2006, ApJ, 646, L107
Chies-Santos A. L., Larsen S. S., Kuntschner H., Anders P., Wehner E. M., Strader J., Brodie J. P., Santos J. F. C., 2011, A&A, 525, A20
Chies-Santos A. L., Larsen S. S., Kissler-Patig M., 2012, MNRAS, 427, 2349
Chiou Y. S., Naoz S., Burkhart B., Marinacci F., Vogelsberger M., 2019, ApJ, 878, L23
Choi J., Dotter A., Conroy C., Cantiello M., Paxton B., Johnson B. D., 2016, ApJ, 823, 102
Choksi N., Gnedin O. Y., Li H., 2018, MNRAS, 480, 2343
Chomiuk L., Strader J., Brodie J. P., 2008, AJ, 136, 234
Cohen J. G., Blakeslee J. P., Ryzhov A., 1998, ApJ, 496, 808
Conroy C., Gunn J. E., 2010, ApJ, 712, 833
Conroy C., Gunn J. E., White M., 2009, ApJ, 699, 486
Conroy C., Villaume A., van Dokkum P. G., Lind K., 2018, ApJ, 854, 139
Cowie L. L., Songaila A., Hu E. M., Cohen J. G., 1996, AJ, 112, 839
Crain R. A. et al., 2015, MNRAS, 450, 1937
D'Antona F., Caloi V., Montalbán J., Ventura P., Gratton R., 2002, A&A, 395, 69
de Boer T. J. L., Fraser M., 2016, A&A, 590, A35
Dotter A. et al., 2010, ApJ, 708, 698
Dotter A., Sarajedini A., Anderson J., 2011, ApJ, 738, 74
El-Badry K., Quataert E., Weisz D. R., Choksi N., Boylan-Kolchin M., 2019, MNRAS, 482, 4528
Elmegreen B. G., 2010, ApJ, 712, L184
Elmegreen B. G., Efremov Y. N., 1997, ApJ, 480, 235
Ferré-Mateu A., Forbes D. A., McDermid R. M., Romanowsky A. J., Brodie J. P., 2019, ApJ, 878, 129
Fontanot F., De Lucia G., Monaco P., Somerville R. S., Santini P., 2009, MNRAS, 397, 1776
Forbes D. A., Bridges T., 2010, MNRAS, 404, 1203
Forbes D. A., Remus R.-S., 2018, MNRAS, 479, 4760
Forbes D. A., Beasley M. A., Brodie J. P., Kissler-Patig M., 2001, ApJ, 563, L143
Forbes D. A. et al., 2017a, AJ, 153, 114
Forbes D. A., Sinpetru L., Savorgnan G., Romanowsky A. J., Usher C., Brodie J., 2017b, MNRAS, 464, 4611
Forbes D. A. et al., 2018, Proc. R. Soc. Lond. Ser. A, 474, 20170616
Foreman-Mackey D., 2016, J. Open Source Software, 1, 24
Foreman-Mackey D., Hogg D. W., Lang D., Goodman J., 2013, PASP, 125, 306

Foreman-Mackey D., Sick J., Johnson B., 2014, Python-fsps: Python Bindings to FSPS (v0.1.1). Available at: https://doi.org/10.5281/zenodo.12157

Gallart C., Bernard E. J., Brook C. B., Ruiz-Lara T., Cassisi S., Hill V., Monelli M., 2019, Nat. Astron., 3, 932

Geisler D., Bica E., Dottori H., Claria J. J., Piatti A. E., Santos J. F. C., Jr, 1997, AJ, 114, 1920

Glatt K. et al., 2008, AJ, 136, 1703

Goudfrooij P., Mack J., Kissler-Patig M., Meylan G., Minniti D., 2001, MNRAS, 322, 643

Goudfrooij P. et al., 2014, ApJ, 797, 35

Gratton R. G., Carretta E., Bragaglia A., Lucatello S., D'Orazi V., 2010, A&A, 517, A81

Gu M. et al., 2018, ApJ, 859, 37

Guérou A., Emsellem E., Krajnović D., McDermid R. M., Contini T., Weilbacher P. M., 2016, A&A, 591, A143

Harris W. E., 1996, AJ, 112, 1487

Harris W. E., 2009, ApJ, 699, 254

Harris W. E., 2010, preprint (arXiv:1012.3224)

Harris W. E., Harris G. L. H., 2002, AJ, 123, 3108

Harris J., Zaritsky D., 2009, AJ, 138, 1243

Harris W. E., Whitmore B. C., Karakla D., Okoń W., Baum W. A., Hanes D. A., Kavelaars J. J., 2006, ApJ, 636, 90

Harris W. E., Blakeslee J. P., Harris G. L. H., 2017, ApJ, 836, 67

Helmi A., Babusiaux C., Koppelman H. H., Massari D., Veljanoski J., Brown A. G. A., 2018, Nature, 563, 85

Hempel M., Hilker M., Kissler-Patig M., Puzia T. H., Minniti D., Goudfrooij P., 2003, A&A, 405, 487

Holtzman J. A. et al., 1992, AJ, 103, 691

Hunter J. D., 2007, Comput. Sci. Eng., 9, 90

Johnson C. I., Pilachowski C. A., 2010, ApJ, 722, 1373

Johnston E. J., Hau G. K. T., Coccato L., Herrera C., 2018, MNRAS, 480, 3215

Jones E. et al., 2001, SciPy: Open Source Scientific Tools for Python. Available at: http://www.scipy.org/

Katz H., Ricotti M., 2014, MNRAS, 444, 2377

Kim J.-h. et al., 2018, MNRAS, 474, 4232

Koleva M., Prugniel P., Ocvirk P., Le Borgne D., Soubiran C., 2008, MNRAS, 385, 1998

Kroupa P., 2001, MNRAS, 322, 231

Kruijssen J. M. D., 2015, MNRAS, 454, 1658

Kruijssen J. M. D., Pfeffer J. L., Crain R. A., Bastian N., 2019a, MNRAS, 486, 3134

Kruijssen J. M. D., Pfeffer J. L., Reina-Campos M., Crain R. A., Bastian N., 2019b, MNRAS, 486, 3180

Kuntschner H., Ziegler B. L., Sharples R. M., Worthey G., Fricke K. J., 2002, A&A, 395, 761

Lamers H. J. G. L. M., Kruijssen J. M. D., Bastian N., Rejkuba M., Hilker M., Kissler-Patig M., 2017, A&A, 606, A85

Larsen S. S., Brodie J. P., Strader J., 2005, A&A, 443, 413

Larsen S. S., Strader J., Brodie J. P., 2012, A&A, 544, L14

Larsen S. S., Brodie J. P., Strader J., 2017, A&A, 601, A96

Layden A. C., Sarajedini A., 2000, AJ, 119, 1760

Leaman R., VandenBerg D. A., Mendel J. T., 2013, MNRAS, 436, 122

Leja J., Johnson B. D., Conroy C., van Dokkum P. G., Byler N., 2017, ApJ, 837, 170

Li H., Gnedin O. Y., 2019, MNRAS, 486, 4030

Li H., Gnedin O. Y., Gnedin N. Y., Meng X., Semenov V. A., Kravtsov A. V., 2017, ApJ, 834, 69

Ma X. et al., 2019, preprint (arXiv:1906.11261)

McDermid R. M. et al., 2015, MNRAS, 448, 3484

Mackereth J. T., Crain R. A., Schiavon R. P., Schaye J., Theuns T., Schaller M., 2018, MNRAS, 477, 5072

Maraston C., Thomas D., 2000, ApJ, 541, 126

Maraston C., Bastian N., Saglia R. P., Kissler-Patig M., Schweizer F., Goudfrooij P., 2004, A&A, 416, 467

Martocchia S. et al., 2018, MNRAS, 473, 2688

Massari D., Posti L., Helmi A., Fiorentino G., Tolstoy E., 2017, A&A, 598, L9

Massari D., Koppelman H. H., Helmi A., 2019, A&A, 630, L4

Milone A. P. et al., 2014, ApJ, 785, 21

Milone A. P. et al., 2018, MNRAS, 481, 5098

Mora M. D., Larsen S. S., Kissler-Patig M., 2008, A&A, 489, 1065

Muratov A. L., Gnedin O. Y., 2010, ApJ, 718, 1266

Myeong G. C., Evans N. W., Belokurov V., Sanders J. L., Koposov S. E., 2018, ApJ, 863, L28

Myeong G. C., Vasiliev E., Iorio G., Evans N. W., Belokurov V., 2019, MNRAS, 488, 1235

Niederhofer F., Hilker M., Bastian N., Silva-Villa E., 2015, A&A, 575, A62

Norris M. A., Sharples R. M., Kuntschner H., 2006, MNRAS, 367, 815

Norris M. A. et al., 2008, MNRAS, 385, 40

Olsen K. A. G., Hodge P. W., Mateo M., Olszewski E. W., Schommer R. A., Suntzeff N. B., Walker A. R., 1998, MNRAS, 300, 665

Oser L., Ostriker J. P., Naab T., Johansson P. H., Burkert A., 2010, ApJ, 725, 2312

Parisi M. C. et al., 2014, AJ, 147, 71

Pastorello N., Forbes D. A., Foster C., Brodie J. P., Usher C., Romanowsky A. J., Strader J., Arnold J. A., 2014, MNRAS, 442, 1003

Peacock M. B., Strader J., Romanowsky A. J., Brodie J. P., 2015, ApJ, 800, 13

Peacock M. B., Zepf S. E., Kundu A., Chael J., 2017, MNRAS, 464, 713

Peacock M. B., Zepf S. E., Maccarone T. J., Kundu A., Knigge C., Dieball A., Strader J., 2018, MNRAS, 481, 3313

Peebles P. J. E., 1984, ApJ, 277, 470

Peng E. W., Ford H. C., Freeman K. C., 2004, ApJ, 602, 705

Pfeffer J., Kruijssen J. M. D., Crain R. A., Bastian N., 2018, MNRAS, 475, 4309

Poci A., McDermid R. M., Zhu L., van de Ven G., 2019, MNRAS, 487, 3776

Portegies Zwart S. F., McMillan S. L. W., Gieles M., 2010, ARA&A, 48, 431

Pota V. et al., 2013, MNRAS, 428, 389

Powalka M. et al., 2016, ApJ, 829, L5

Puzia T. H., Zepf S. E., Kissler-Patig M., Hilker M., Minniti D., Goudfrooij P., 2002, A&A, 391, 453

Puzia T. H., Kissler-Patig M., Thomas D., Maraston C., Saglia R. P., Bender R., Goudfrooij P., Hempel M., 2005, A&A, 439, 997

Qu Y. et al., 2017, MNRAS, 464, 1659

Recio-Blanco A., Aparicio A., Piotto G., de Angeli F., Djorgovski S. G., 2006, A&A, 452, 875

Reina-Campos M., Kruijssen J. M. D., Pfeffer J. L., Bastian N., Crain R. A., 2019, MNRAS, 486, 5838

Rodriguez-Gomez V. et al., 2016, MNRAS, 458, 2371

Sánchez-Blázquez P. et al., 2006, MNRAS, 371, 703

Schaye J. et al., 2015, MNRAS, 446, 521

Schiavon R. P., 2007, ApJS, 171, 146

Schlafly E. F., Finkbeiner D. P., 2011, ApJ, 737, 103

Schuster W. J., Moreno E., Nissen P. E., Pichardo B., 2012, A&A, 538, A21

Searle L., Zinn R., 1978, ApJ, 225, 357

Sesto L. A., Faifer F. R., Smith Castelli A. V., Forte J. C., Escudero C. G., 2018, MNRAS, 479, 478

Shapiro K. L., Genzel R., Förster Schreiber N. M., 2010, MNRAS, 403, L36

Sharina M. E., Afanasiev V. L., Puzia T. H., 2006, MNRAS, 372, 1259

Snaith O. N., Haywood M., Di Matteo P., Lehnert M. D., Combes F., Katz D., Gómez A., 2014, ApJ, 781, L31

Sohn S. T., Watkins L. L., Fardal M. A., van der Marel R. P., Deason A. J., Besla G., Bellini A., 2018, ApJ, 862, 52

Spitler L. R., Forbes D. A., 2009, MNRAS, 392, L1

Spolaor M., Forbes D. A., Proctor R. N., Hau G. K. T., Brough S., 2008, MNRAS, 385, 675

Strader J., Brodie J. P., Cenarro A. J., Beasley M. A., Forbes D. A., 2005, AJ, 130, 1315

Thomas D., Maraston C., Bender R., 2003, MNRAS, 339, 897

Thomas D., Maraston C., Korn A., 2004, MNRAS, 351, L19

Thomas D., Maraston C., Bender R., Mendes de Oliveira C., 2005, ApJ, 621, 673

Trenti M., Padoan P., Jimenez R., 2015, ApJ, 808, L35

Usher C. et al., 2012, MNRAS, 426, 1475

Usher C. et al., 2015, MNRAS, 446, 369

Usher C. et al., 2017, MNRAS, 468, 3828

Usher C. et al., 2019, MNRAS, 482, 1275

VandenBerg D. A., Brogaard K., Leaman R., Casagrande L., 2013, ApJ, 775, 134

van den Bergh S., 1969, ApJS, 19, 145

van den Bergh S., 1981, A&AS, 46, 79

van der Walt S., Colbert S. C., Varoquaux G., 2011, Comput. Sci. Eng., 13, 22

Villanova S., Geisler D., Gratton R. G., Cassisi S., 2014, ApJ, 791, 107

Villaume A., Romanowsky A. J., Brodie J., Strader J., 2019, ApJ, 879, 45

Whitmore B. C., Schweizer F., Leitherer C., Borne K., Robert C., 1993, AJ, 106, 1354

Wilkinson D. M., Maraston C., Goddard D., Thomas D., Parikh T., 2017, MNRAS, 472, 4297

Worthey G., 1994, ApJS, 95, 107

Worthey G., Faber S. M., Gonzalez J. J., Burstein D., 1994, ApJS, 94, 687

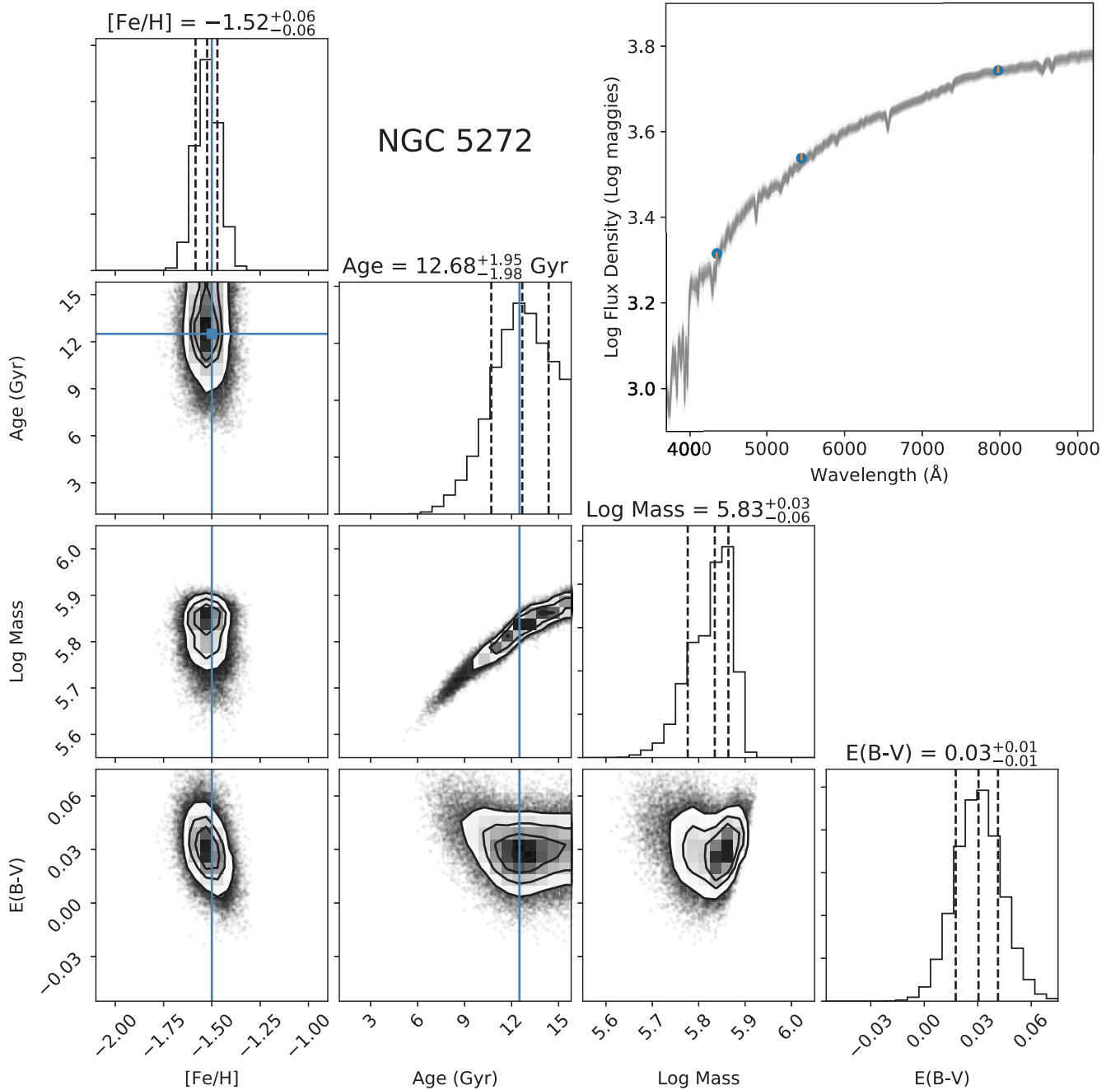# APPENDIX: EXAMPLE POSTERIOR DISTRIBUTIONS

Figure A1. Posterior distributions of metallicity, age, mass, and reddenings for the MW GC NGC 5272. The metallicity from the 2010 edition of the Harris (1996, 2010) catalogue and resolved colour–magnitude age from Dotter et al. (2010) are overplotted in blue. In the top left, we plot the spectral energy distributions calculated by FSPS for 256 points drawn at random from the posterior distribution in grey, the median colours of the posterior distribution as blue circles, and the observed photometry as orange error bars.
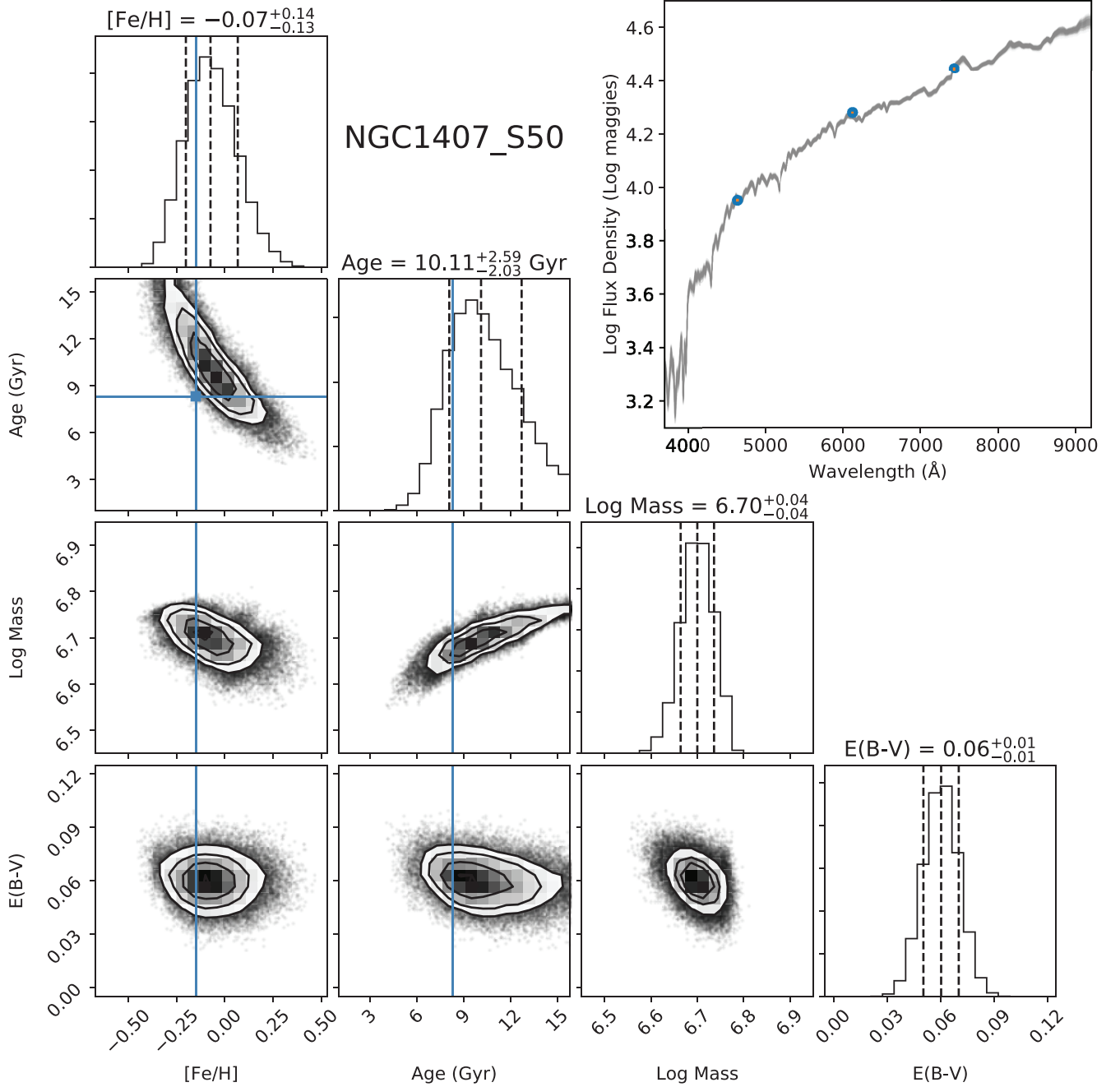
Figure A2. Posterior distributions of metallicity, age, mass, and reddenings for the NGC 1407 GC NGC 1407_S50. The metallicity and age based on the analysis of Lick indices by Cenarro et al. (2007) are overplotted in blue. In the top left, we plot the spectral energy distributions calculated by FSPS for 256 points drawn at random from the posterior distribution in grey, the median colours of the posterior distribution as blue circles, and the observed photometry as orange error bars.

This paper has been typeset from a TEX/LATEX file prepared by the author.